ACS APPLIED MATERIALS & INTERFACES

www.acsami.org Research Article

Electrostatic Air Filtration by Multifunctional Dielectric Heterocaking Filters with Ultralow Pressure Drop

Enze Tian, Fanxuan Xia, Jiandong Wu, Yinping Zhang, Ju Li, Hao Wang,* and Jinhan Mo*

Cite This: *ACS Appl. Mater. Interfaces* 2020, 12, 29383–29392 Read Online

ACCESS | Metrics & More | Article Recommendations | Supporting Information

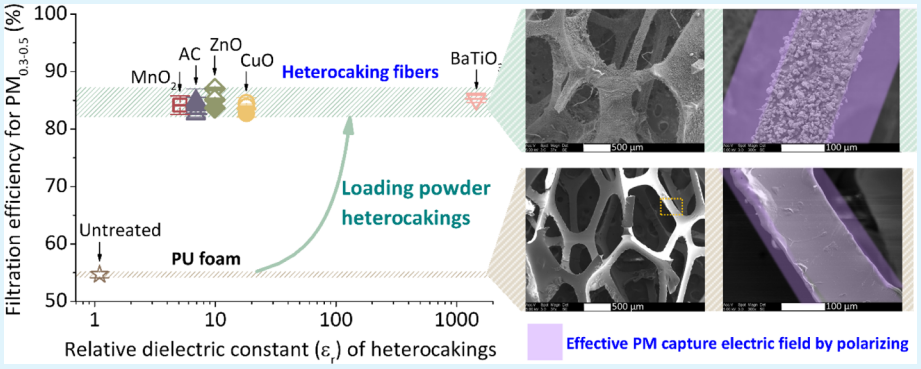

ABSTRACT: In air filtration, for creating healthy indoor air, there is an intrinsic conflict between high filtration efficiency and low wind pressure drop. In this study, we overcame this conflict by developing new dielectric heterocaking (HC) filters, in which high relative dielectric constant (ε_r) materials were heterogeneously loaded on traditional polymer fibers. The dielectric HC filters in an electrostatic polarizing field generate a great amount of charges on their surface, leading to a strong attraction to precharged aerosol particles, and result in high filtration efficiency. Observing *via* a charged coupled device camera, the migration speed of aerosol smoke particles toward the polarized HC fiber exceeded those toward the unpolarized HC fiber by a factor of 6. We loaded high-ε_r HCs including manganese dioxide (MnO_2), activated carbon, zinc oxide (ZnO), copper oxide (CuO), and barium titanate ($BaTiO_3$) on polyurethane foams using a fast and large-scale roll-to-roll gel squeezing method. Based on the experimental results, when HCs had a ε_r larger than 5.1, an increased ε_r did not benefit electrostatic filtration efficiency for aerosol particles much, but resulted in a larger net ozone production. We suggested a MnO_2-HC filter for efficient and multifunctional filtration of indoor particles, ambient ozone, and formaldehyde with only 3.8 Pa pressure drop at 1.1 m/s filtration velocity. This efficient and cost-effective dielectric HC filter opens a new avenue for the design of multifunctional filters, which will facilitate its large-scale production and commercial application in the ventilation system for healthy buildings.

KEYWORDS: *indoor air quality, particulate matter, ozone, formaldehyde, CCD camera, polyurethane foam*

1. INTRODUCTION

Airborne pollutants including particulate matter (PM), ozone, and formaldehyde pose serious health threats to the public. Exposure to PM increases the risk of dementia,[1,2] diseases of the respiratory and cardiovascular systems,[3,4] and mortality.[5,6] Submicrometer particles (PM_1) are more harmful than micrometer-sized particles because they can go deeper into the human respiratory system.[7−9] Besides PM, ambient ozone exposure contributes to the risk of respiratory, cardiovascular, and circulatory mortality.[10,11] Ozone also reacts with certain indoor chemical pollutants to generate secondary ultrafine particles, which have been associated with adverse health effects.[12] Furthermore, formaldehyde, one of the most common volatile organic compounds (VOCs) in Chinese residences, has been classified as carcinogenic and teratogenic by the World Health Organization.[13] Specifically, for adults in urban China, formaldehyde has become the most significant contributing pollutant to inhalation cancer risk.[14] Therefore, the development of high-efficiency air filtration technologies that can simultaneously remove hazardous PM, ozone, and formaldehyde is a critical need for public health.[15,16]

In addition, climate emergency is another pressing issue. Scientists have warned that the world should quickly implement massive energy efficiency and conservation practices for humanity and the environment.[17] However, there is an intrinsic

Received: April 22, 2020
Accepted: June 5, 2020
Published: June 5, 2020

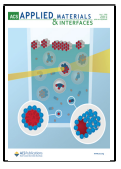

https://dx.doi.org/10.1021/acsami.0c07447
ACS Appl. Mater. Interfaces 2020, 12, 29383−29392

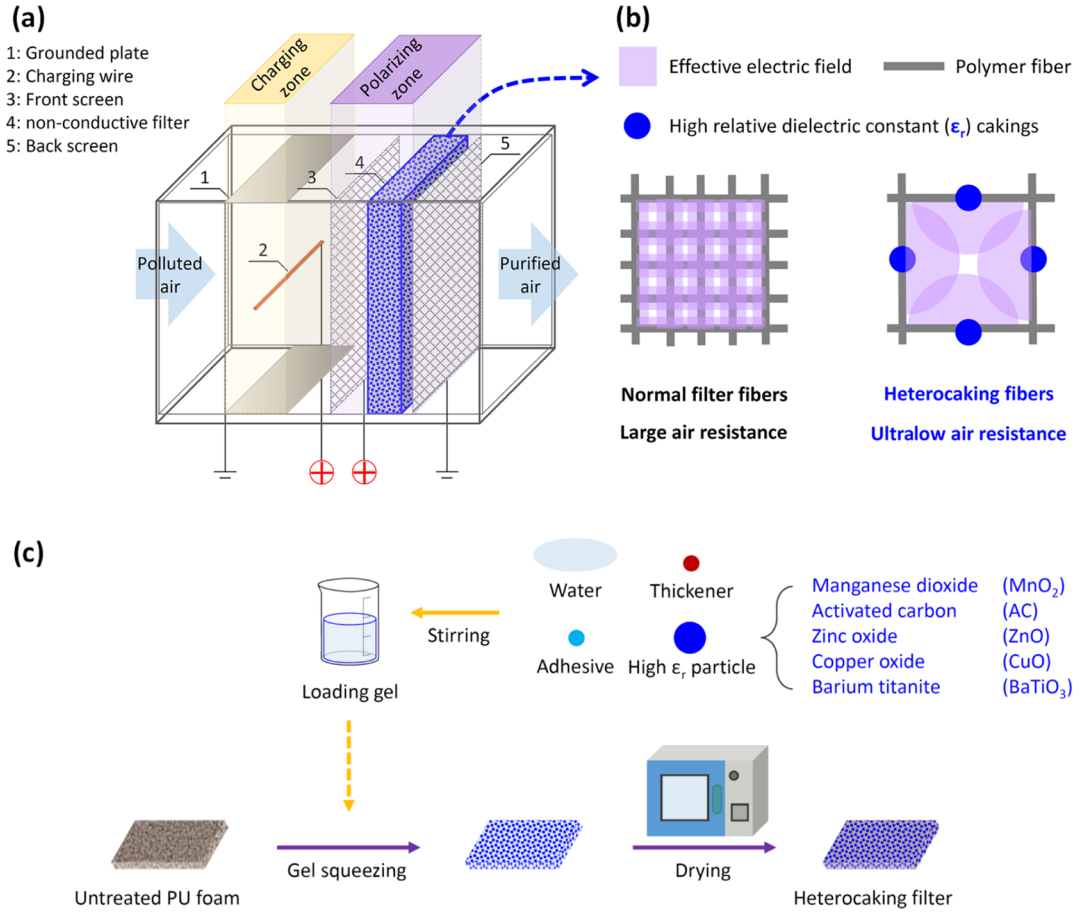

Figure 1. (a) Schematic of the electrostatically assisted heterocaking (EAHC) air filter module; (b) schematic of heterocaking (HC) fibers in a polarizing field compared with normal filter fibers; and (c) preparation process of HC filters by a fast and large-scale roll-to-roll gel squeezing method.

conflict that high-efficiency air filtration usually has large air resistance and costs up to 50% power consumption of the driving fans.[18,19] Developing efficient airborne pollutant filtration technologies with minimal pressure drop and energy consumption is a great challenge. To accomplish this, combining continuous electrostatic effects with fibrous filtration has been proposed.

Wang *et al.* assembled electret PVDF/PTFE nanofibrous membranes, which had a highest filtration efficiency of 99.972% for $PM_{2.5}$ (PM with aerodynamic diameters less than 2.5 μm) and a pressure drop of 57 Pa at 5.3 cm/s air velocity.[20] Several researchers enhanced the filtration efficiency of commercial filters by operating an ionizer in front of them.[21−25] In these studies, the largest filtration efficiency enhancement was from 5 to 73% for 0.5 μm particles, with 82 Pa pressure drop at 1.1 m/s air velocity.[21] In these studies, either particles or filters were charged, and so the electrostatic filtration efficiency enhancement was limited. Some researchers installed particle prechargers before conductive filters to strengthen the electrostatic effect.[26−29] In these studies, the highest filtration efficiency was 99.99% for 0.03−0.4 μm particles with 4.9 Pa pressure drop at 0.1 m/s face air velocity.[27,28] However, the electrostatic shielding limits these filters' dust-holding capacity because there is no electric force inside the conductive filter material.

Therefore, synergistic particle precharging and nonconductive filter polarization was proposed as a promising way to achieve high efficiency, low pressure drop, and large particle capacity at the same time.[30−35] Approaching to the minimal pressure drop, Tian and Mo developed a new structure for the electrostatically assisted air (EAA) coarse filter device, in which corona charging and polarizing fields are independently controlled and optimized to realize a higher filtration efficiency. The device increased the single-pass filtration efficiency for 0.3−0.5 μm particles of a coarse filter from 0.4 to 99.0% with 21.0 Pa pressure drop at 1.2 m/s filtration velocity.[31] However, for these studies, the external voltages were limited by the problems such as dangerous air break down and hazardous ozone byproducts. Therefore, when approaching to a further lower pressure drop, a new filter material with desirable dielectric properties should be designed to replace the commercial filters. In this way, the filter can have a better electrostatic response to the external fields and achieve a higher filtration efficiency without further lifting external voltages. Moreover, when the new filter material is made of an adsorbent or catalyst, airborne ozone and formaldehyde might be simultaneously removed together with particles.

In this study, we aimed to optimize the material to make a multifunctional filter to lower the pressure drop further and maintain high air pollutant removal efficiencies. To achieve that, we proposed and fabricated new electrostatically assisted heterocaking (EAHC) filters by using polyurethane (PU) foams with extremely low pressure drop as base filters and heterogeneously loading high-ε_r heterocakings (HCs) [manganese dioxide, activated carbon (AC), zinc oxide, copper oxide, and barium titanate] on them. From the observation *via* a charged coupled device (CCD) camera, we found that the HCs on the fiber surfaces in an electrostatic polarizing field have

https://dx.doi.org/10.1021/acsami.0c07447
ACS Appl. Mater. Interfaces 2020, 12, 29383−29392

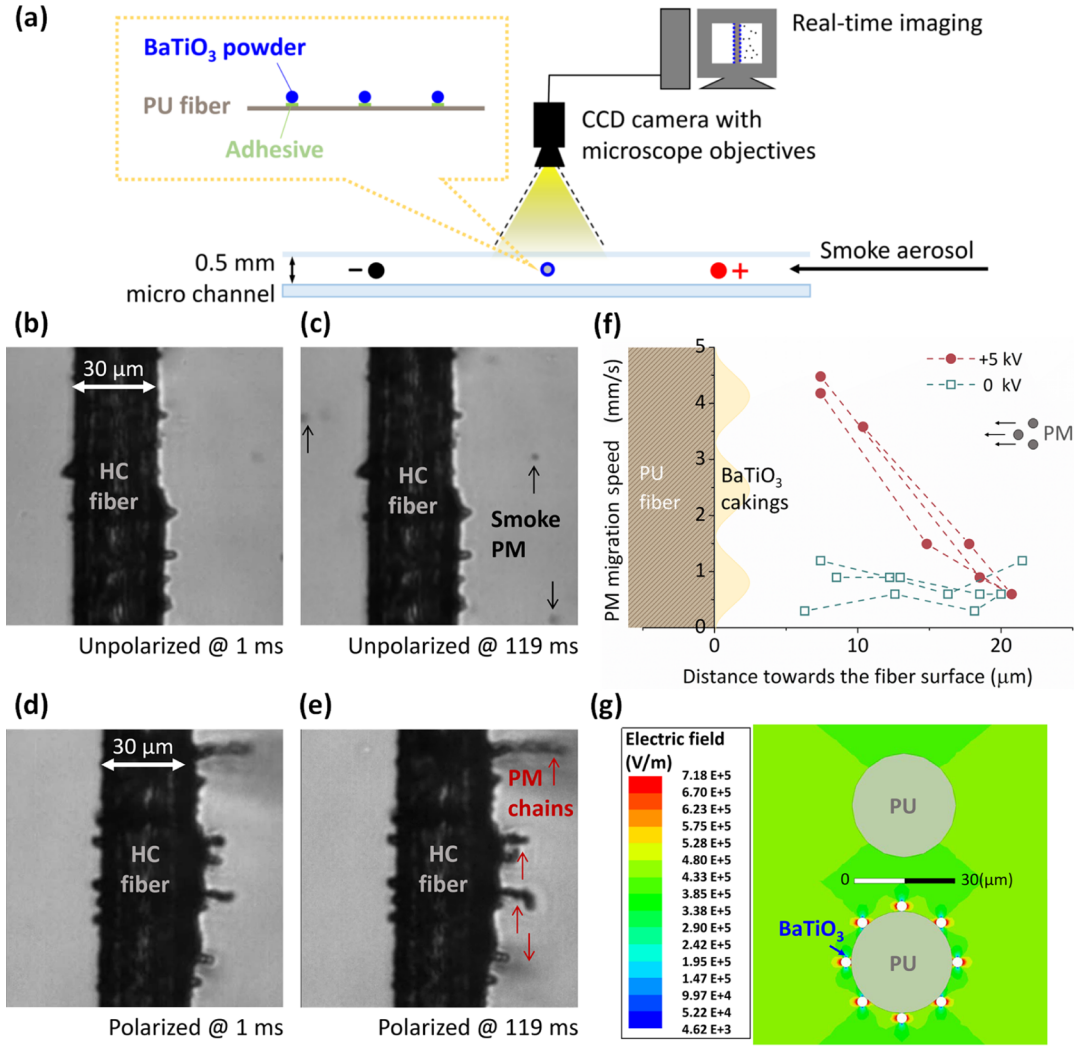

Figure 2. (a) Schematic of an *in situ* CCD observation platform. Photographs of smoke particle migration behavior toward the heterocaking (HC) fiber caught by the CCD camera when (b) no voltage is applied to the charging wire at 1 ms; (c) no voltage is applied to the charging wire at 119 ms; (d) +5 kV is applied to the charging wire at 1 ms; and (e) +5 kV is applied to the charging wire at 119 ms. (f) Particle migration speed along the distance toward the HC fiber surface when no voltage (square hollow) or +5 kV (circle solid) is applied to the charging wire. The electric field around the polarized (g) PU fiber and HC ($BaTiO_3$ loaded PU) fiber simulated by Maxwell 3D.

strong attractions to precharged aerosol particles. Quantitative experiments revealed that the EAHC filter has not only high single-pass filtration efficiency for airborne PM, ozone, and formaldehyde but also low pressure drop and low power dissipation. This efficient and cost-effective dielectric HC filter opens a new avenue for the design of multifunctional filters, which will facilitate its large-scale production and commercial application in the ventilation system for healthy buildings.

2. THEORETICAL BASIS

The schematic of the EAHC air filter module is shown in Figure 1a. The polluted air is driven into the air duct and first precharged by a wire-to-plate discharger (in the charging zone) and then driven toward the filter with a polarizing field through it (in the polarizing zone). The polarizing field induces charges on the surfaces of the dielectric filter material.[36] The charged particles are then captured by the polarized fibers owing to the electric force F_e (N) between them[37]

$$F_e = E_p q\left[1 + \left(\frac{\varepsilon_r - 1}{\varepsilon_r + 1}\right)\frac{{d_f}^2}{4R^2}\right] \quad (1)$$

where E_p is the external polarizing field intensity (V/m); q is the charge (C) of a particle; ε_r is the relative dielectric constant of the fiber; d_f is the fiber diameter (μm); and R is the distance (μm) between the centerline of the fiber and the particle. The larger the F_e is, the higher the filtration efficiency of the EAHC air filter module will be.

As shown in Figure 1b, the area of the effective electric field (purple zone) around each normal filter fiber is limited. It requires the gaps among fibers to be relatively small; otherwise, the airborne particles will easily penetrate through the filter. The heterogeneous location of high-ε_r HCs (the blue dots in Figure 1b) will form a larger electric field. Therefore, the gap between HC fibers can be larger than that between the normal filter fibers, resulting in a lower pressure drop at the same filtration efficiency level. Furthermore, when the loaded HCs are made of an adsorbent or catalyst, some indoor hazardous gas, such as ozone and formaldehyde, is expected to be removed.

https://dx.doi.org/10.1021/acsami.0c07447
ACS Appl. Mater. Interfaces 2020, 12, 29383−29392

3. EXPERIMENTAL SECTION

3.1. Materials. PU foams (thickness: 8 mm, filter porosity: 35 ppi, ~1 mm pore diameter) and AC powder and granules were obtained from Zhongshan Topg Ecology Tech Co. Ltd., China. PU fibers were purchased from Shanghai Yanya Ecology Tech Co. Ltd., China. Manganese dioxide (MnO_2) powder (10 μm particle size, >90%), zinc oxide (ZnO) powder (<100 nm particle size, 99.7%), copper oxide (CuO) powder (<50 nm particle size, 99.5%), and barium titanate ($BaTiO_3$) powder (<2 μm particle size, 99.9%) were obtained from Sigma-Aldrich Inc., US. Vinyl acetate−ethylene (VAE) copolymer emulsion [VINNAPAS EP 705A (ULS)] was obtained from Wacker Chemical Corp., US. Sodium carboxymethyl cellulose (CMC-Na) was obtained from Guangzhou Suixin Chemical Industrial Co. Ltd., China. The 502 cyanoacrylate instant adhesive super glue (502 glue) was purchased from ABN BOND Co., Ltd., China.

3.2. *In Situ* CCD Observation of Particle Deposition on HC Fibers. A PU fiber with approximately 30 μm diameter was dipped into 502 glue and $BaTiO_3$ powder in sequence and dried naturally in air. After 10 min, $BaTiO_3$ HCs were firmly loaded on the PU fiber. As shown in Figure 2a, the HC fiber was placed in the middle of a microchannel made of glass slides having a 0.5 mm gap. Two tungsten wires (0.1 mm diameter) were placed 6 mm upstream and downstream the HC fiber, respectively. The upstream wire was connected to a 0 to +10 kV adjustable high voltage direct current (HVDC) power supply (P10, GENVOLT, China), and the downstream wire was connected to the ground. We used smoke aerosol generated by a burning cigarette as the pollutant source and injected the particles into the microchannel using a Pasteur pipette. On applying +5 kV to the charging wire, corona discharge happened and the particles got charged. The wires at the same time formed a polarizing electric field between them through the HC fiber. The microchannel was placed under an optical microscope (50×), and real-time images of fiber capturing particles were recorded using a CCD camera (403 fps).

3.3. Electrostatic Simulation. The electric field around the polarized fibers was computed using a finite-volume solver, Maxwell 3D, developed by Ansoft Corp. Two two-dimensional models (PU fibers with and without $BaTiO_3$ HC loading) were constructed. The fibers were placed at the center of two parallel 0.1 mm × 12 mm stainless steel plates, one of which was applied +5 kV voltage, while another was connected to the ground. The gap between the two plates was 12 mm and was filled with air medium. The diameters of the fibers and HCs were 30 and 3 μm, respectively. The relative dielectric constants (ε_r) of the fibers and HCs were 1.1 and 1450, respectively, as shown in Table 1.

3.4. Fabrication of HC Filters. As shown in Figure 1c, the HC filter preparation process includes (1) preparing loading powders by sieving the MnO_2, AC, ZnO, CuO, and $BaTiO_3$ powders using 100 mesh; (2) preparing the adhesive gel by mixing the CMC-Na (as the thickener), VAE copolymer emulsion (as the adhesive), and water at a mass ratio of 1:50:100 under moderate stirring until they dissolved; (3) preparing loading gels by mixing each kind of loading powder or granule and adhesive gel at a mass ratio of 1:3, 1:2, or 1:1 with a stirring speed of 500 rpm for 10 min; (4) dipping PU foams into loading gels and squeezing redundant loading gels by a double roller; and (5) drying the foams in an oven at 80 °C for 180 min. The HC filters were washed by hands, as demonstrated in the Supporting Information Video S1, and there was no visible unloaded HC in the water after washing. Table 1 lists the detailed fabrication parameters of the obtained filters.

3.5. Characterization and Performance Test. Scanning electron microscopy (SEM) images and elementary composition of the filters were obtained using an electron microscope (Nova NanoSEM 450, FEI Inc., USA) equipped with an energy-dispersive spectrometer (EDS) detector. Brunauer−Emmett−Teller (BET) gas physisorption measurements were conducted to examine the porous nature of the HC filters. The performance of the EAHC air filtration module was evaluated following similar procedures as in previous studies.[44] The experimental details are introduced in the Supporting Information. In brief, ambient PM, ambient ozone, and formaldehyde generated by a syringe pump injector[45] were used as the pollutant source. The air filtration velocities across the filters (v_{filt}) were controlled at 1.1 m/s, except for formaldehyde removal performance at 0.35 m/s.

Table 1. Fabrication Parameters of the PU Foam and HC Filters

filters	loading materials	ε_r of loading materials[a]	loading materials/adhesive mass ratio	net loading amount, g/m^2
PU	none	1.1		0[b]
MnO_2-3	MnO_2 (powder)	5.1	1:3	289
AC-1	AC (powder)	6.9	1:1	213
AC-2	AC (powder)	6.9	1:2	172
AC-3	AC (powder)	6.9	1:3	133
gAC-1	AC (granules)	6.9	1:1	782
gAC-2	AC (granules)	6.9	1:2	653
gAC-3	AC (granules)	6.9	1:3	583
ZnO-1	ZnO (powder)	9.9	1:1	433
ZnO-2	ZnO (powder)	9.9	1:2	317
ZnO-3	ZnO (powder)	9.9	1:3	300
CuO-1	CuO (powder)	18.1	1:1	446
CuO-2	CuO (powder)	18.1	1:2	435
CuO-3	CuO (powder)	18.1	1:3	385
$BaTiO_3$-3	$BaTiO_3$ (powder)	1450	1:3	462

[a]Relative dielectric constant obtained from the literature.[38−43] [b]Weight of the bare PU foam was 156 g/m^2.

Following the calculation method in the Supporting Information, we obtained the single-pass filtration efficiency $\eta(d_p)$ of particles with a certain size of d_p (μm), the single-pass filtration efficiency of formaldehyde η_{HCHO}, net ozone production ΔC_{ozone} (ppb), and the total power consumption of the EAHC air filter module P_{total} (W/m^2) (including the power consumption of the HVDC power supply P_{supply} and the driving fan P_{fan}). We used quality factor, QF (Pa^{-1}), and comprehensive quality factor, CQF (Pa^{-1}), to evaluate the overall particle removal performance of the EAHC air filter device. QF considers filtration efficiency and pressure drop of the filter,[46] and CQF considers filtration efficiency, pressure drop, and power consumption of the whole filter module.[29]

4. RESULTS AND DISCUSSION

4.1. *In Situ* Observation and Electrostatic Simulation. As a proof of concept, Figure 2b−e and Supporting Information Videos S2 and S3 reveal the particle capturing behaviors of the HC fiber recorded using the CCD camera. When no voltage was applied to the charging wire, the smoke particles passed by the HC fiber with a slow velocity (~0.7 mm/s). When +5 kV was applied to the charging wire, the smoke particles deposited to the HC fiber fast, forming particle chains specifically upon the $BaTiO_3$ cakings. As shown in Figure 2f, the particle migration speed increased from ~0.6 to ~4.1 mm/s when particles were moving toward the HC fiber from ~20 to ~8 μm away.

The reason for fast deposition of particles specifically onto the $BaTiO_3$ cakings in a polarizing field was that the electric field intensity near the $BaTiO_3$ cakings was far stronger than that near the bare PU fiber. For example, as shown in Figure 2g, the

https://dx.doi.org/10.1021/acsami.0c07447
ACS Appl. Mater. Interfaces 2020, 12, 29383−29392

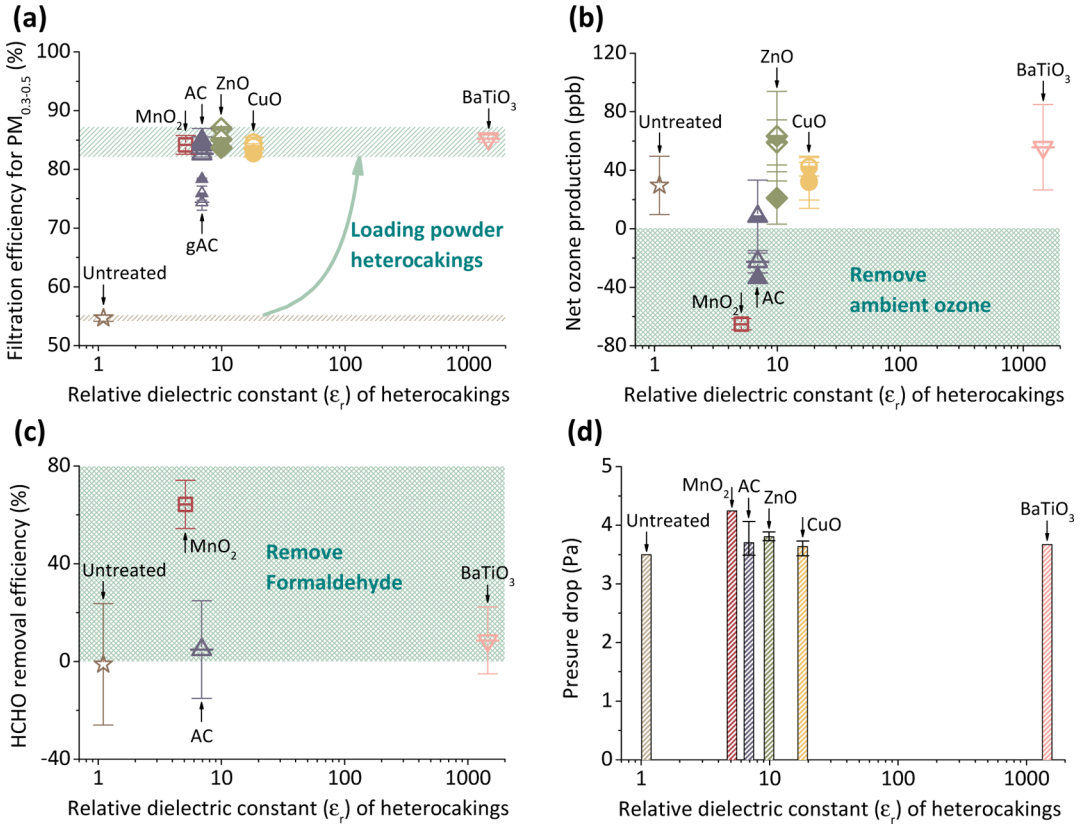

Figure 3. Multifunctional air purification performances of electrostatically assisted PU foam and HC filters. (a) Single-pass filtration efficiencies for 0.3−0.5 μm particles ($PM_{0.3-0.5}$); (b) net ozone production; (c) single-pass removal efficiency for formaldehyde; (d) pressure drop. Hollow, semi-solid, and solid dots represent particle/adhesive mass ratio being 1:3, 1:2, and 1:1, respectively. AC represents powdered activated carbon, and gAC represents granular activated carbon. The error bars in the figures (a−c) are the standard deviations of six observations of the experiments; in figure (d) are the variations of results for three filters loaded with different particle/adhesive mass ratios.

highest electric field intensities near the bare PU and the $BaTiO_3$ cakings were 4.22×10^5 and 9.34×10^5 V/m, respectively. Both the *in situ* observation and electrostatic simulation results revealed that loaded with high-ε_r HCs, the polarized fibers have a stronger attraction to aerosol particles and result in higher filtration efficiency.

4.2. Morphologies and Components of HC Filters. Figures S1−S3 and Table S1 in the Supporting Information show the SEM images, EDS elemental analysis, pore volume distribution, and specific surface area of the filters listed in Table 1, respectively. The HCs were mostly loaded on the surface of PU foam fiber, but occasionally formed some bulk, blocking the pores of PU foams. A different loading material and particle/adhesive mass ratio did not make much difference in the macromorphologies of the HC filters. All filters showed macroscopic pore sizes (~1 mm), ensuring that HC filters in this study had ultralow pressure drops. However, for AC loading, as shown in Figures S1c−h and S3 in the Supporting Information, use of powder-loaded AC particles formed a more uneven HC distribution on the PU foam and exhibited a wider pore width range (micropores and mesopores) than when granule-shaped AC particles (micropores) were used, although they had a similar BET surface area as shown in Table S1 in the Supporting Information.

4.3. Performance for Submicrometer Particle Removal. Because ambient aerosols were the pollutant source, air temperature and relative humidity were not controlled but just recorded as 33.6−36.1 °C and 23.4−29.0%, respectively. The size distributions of the particulate pollutant source are shown in Figure S4 in the Supporting Information.

Figures 3a and S5a in the Supporting Information show the single-pass filtration efficiency for $PM_{0.3-0.5}$ and $PM_{0.5-1}$ (PM with aerodynamic diameters of 0.3−0.5 and 0.5−1 μm) of the electrostatically assisted PU foam and HC filters when charging voltage (U_c) and polarizing voltage (U_p) were set at +9.0 and +21.0 kV, respectively. It is worth noting that all filters in this study had nearly no efficiency for $PM_{0.3-0.5}$ because of their large pore size (~1 mm). By applying voltages to the filtration module, the single-pass filtration efficiency of the electrostatically assisted PU foam increased to 54.7% for $PM_{0.3-0.5}$. Further, by loading HCs onto the PU foams, the filtration efficiency of the EAHC filters increased obviously to 74.4−87.0% for $PM_{0.3-0.5}$. It was as expected in the results of *in situ* observation and electrostatic simulation that after loading a PU fiber with high-ε_r HCs, the polarized HC fiber would have a stronger attraction to precharged aerosol particles and therefore resulted in higher filtration efficiency.

Figure 3a shows that the shape of the loading particles (powder or granules) has the greatest influence on the filtration efficiency of the EAHC filters, compared to the particle/adhesive mass ratio (loading amount) and the material of the loading particles. For example, powdered AC-loaded filters had a higher average efficiency (84.0% for $PM_{0.3-0.5}$) than granular AC-loaded filters (76.2% for $PM_{0.3-0.5}$). Besides, AC derived from different materials with different treatment conditions

https://dx.doi.org/10.1021/acsami.0c07447
ACS Appl. Mater. Interfaces 2020, 12, 29383−29392

would differ in ε_r,[40] leading to the differences in electrostatic filtration efficiency for ambient particles.

The HC loading amount did not much influence the electrostatic filtration efficiency for submicrometer particles. For example, 583 to 782 g/m^2 loading of AC granules made single-pass filtration efficiencies for $PM_{0.3-0.5}$ varied from 74.4 to 78.4%, 133 to 213, 300 to 433, and 385 to 446 g/m^2 powder AC, ZnO, CuO loading made single-pass filtration efficiencies for $PM_{0.3-0.5}$ varied from 82.6 to 84.5, 83.7 to 87.0, and 82.7 to 84.6%, respectively. Noting that the weight of the bare PU foam was 156 g/m^2, we suspected that when HC loading amount was in the order of magnitude with the weight of the substrate filter, the loading amount's influence on the electrostatic filtration efficiency would be limited.

Moreover, the HC material (ε_r > 5.1) did not have much influence on electrostatic filtration efficiency for submicrometer particles either. The single-pass filtration efficiencies of powder-loaded HC filters for $PM_{0.3-0.5}$ varied only from 82.6 to 87.0%, although the ε_r of the HCs varied from 5.1 to 1450. The following two reasons might explain such a phenomenon. (1) The high-ε_r loading particles were mixed with the adhesive and might be covered with the adhesive, and so the ε_r of the loaded HC fibers may not be approximate to the corresponding loading particles', but can be estimated to the adhesives'. (2) Based on eq 1, we used parameters obtained from our experiments and literature (see in Tables 1 and 2) to calculate the theoretical electric force (F_e) of the five powder-loaded HC filters. When ε_r changes from 5.1 to 1450, F_e changes from 0.020 to 0.024 nN, indicating that HC does not need an extremely large ε_r to achieve a high electrostatic filtration efficiency for ambient particles.

Table 2. Parameters Used for F_e Calculation

E_p, V/m	q, C	ε_r	d_f, μm	R, μm
8.75×10^5	1.37×10^{-17}[a]	as in Table 1	150[b]	75.2[c]

[a]Calculated from literature.[47] [b]Estimated from Figure S1 in the Supporting Information. [c]Considering $PM_{0.3-0.5}$ with an average diameter value of 0.4 μm.

It is worth noting that by loading PU foams with high-ε_r HCs, the pressure drop increased only from 3.5 to 4.2 Pa (as shown in Figure 3d). As shown in Figure S1 in the Supporting Information, the HC particles were much smaller than the pore size of the PU foams and were only loaded slightly on the surface of PU foam fibers. Therefore, they would not significantly increase the pressure drop of the PU foam. With much enhanced single-pass filtration efficiencies and nearly no increased pressure drops, the HC filters showed higher QFs than the bare PU foam. As shown in Figure S4c in the Supporting Information, QF for $PM_{0.3-0.5}$ increased from 0.226 to 0.539 Pa^{-1} after loading PU foams with high-ε_r HCs, indicating that the HCs do a lot good in improving PU foam to an energy-efficient filtration material. Moreover, while considering power consumption of the EAHC air filtration module, as shown in Figure S4b,d in the Supporting Information, CQF for $PM_{0.3-0.5}$ increased from 0.173 to 0.411 Pa^{-1} after loading PU foams with high-ε_r HCs.

4.4. Performance for Ozone and Formaldehyde Removal. Figure 3b shows the net ozone production of the EAHC air filtration module when U_c and U_p are controlled at +9.0 and +21.0 kV, respectively. On using bare PU, there was 29.7 ppb net ozone production (air temperature: 33.6−36.1 °C, relative humidity: 23.4−29.0%). On loading the PU foam with MnO_2 and powdered and granular AC, the net ozone productions decreased to −65.2, −15.9, or −44.2 ppb, respectively, thus preventing the module from not only producing but also removing the hazardous ozone from the ambient air. Considering that the average inlet ozone concentration was 121.3 ppb, the ozone removal efficiencies of MnO_2, powdered or granular AC-loaded filters were 53.8, 13.1, and 36.4%, respectively. It is because during the precharging process, not only aerosol particles but also the ozone molecules are charged.[48] These charged ozone molecules then are captured by polarized fibers owing to the electric force. When MnO_2 HCs are loaded on the fibers, they act as the catalyst in decomposition of the ambient ozone,[49] while AC HCs act as the adsorbent for adsorbing ambient ozone and decompose ozone by some active groups on it.[50] Granular AC-loaded filters had higher ozone removal potential than those containing powdered AC, owing to their greater loading amount

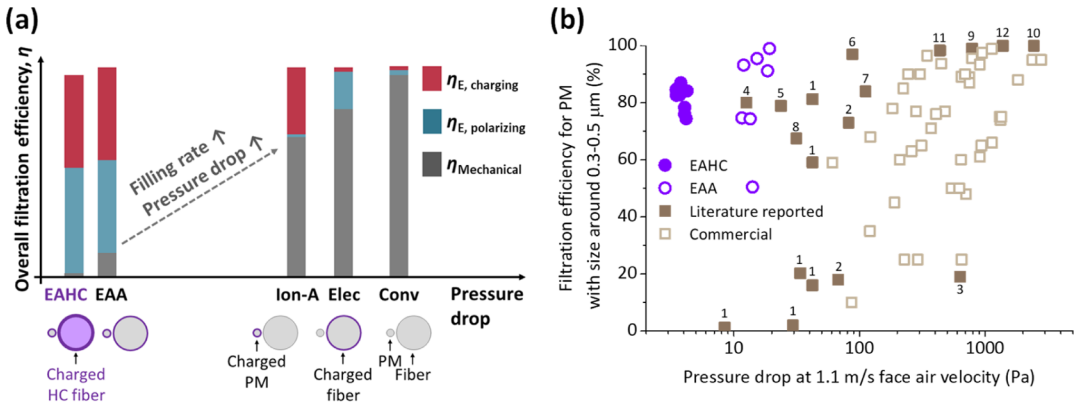

Figure 4. Single-pass filtration efficiency and pressure drop (Δp) of five filters. (a) Schematic (EAHC is electrostatically assisted air filter with HC coating; EAA is electrostatically assisted air filter without HC coating; Ion-A is ion assisted air filter; Elec is electret filter; Conv is conventional filter based mostly on mechanical filtration effect; $\eta_{E,\ charging}$ and $\eta_{E,\ polarizing}$ are the filtration efficiencies contributed by the charged PM and the polarized filter, respectively; $\eta_{mechanical}$ is the filtration efficiency contributed by mechanical effect); (b) real data including EAHC filters in this study, EAA filters,[31] other literature reported filters (1,[54] 2,[21] 3,[22] 4,[24] 5,[29] 6,[33] 7,[34] 8,[25] 9,[55] 10,[56] 11,[57] and 12[58]), and commercial filters.[59] If the experiments in the literature were not conducted at 1.1 m/s face air velocity, we calculated the equivalent Δp by assuming that Δp was proportional to face air velocity.[18]

https://dx.doi.org/10.1021/acsami.0c07447
ACS Appl. Mater. Interfaces 2020, 12, 29383−29392

(as shown in Table 1) and larger surface area (as shown in Table S1 in the Supporting Information). However, on loading the PU foam with ZnO, CuO, or $BaTiO_3$, the net ozone productions increased to 47.8, 35.6, or 55.8 ppb, respectively. We suspected that when the HCs had such high ε_r to generate a large amount of charge on their surfaces, local microdischarging might happen in the polarized HC filters. Therefore, high ε_r of the HCs without catalyst or adsorbent function would result in a large net ozone production.

Figure 3c shows the single-pass removal efficiency for formaldehyde of the EAHC air filter module when U_c and U_p were controlled at +9.0 and +10.0 kV, respectively. The average inlet formaldehyde concentration was 0.987 ppm (air temperature: 29−31 °C, relative humidity: 20−30%). Because most of the HC filters showed nearly no removal efficiency for formaldehyde, we only showed the results for PU, MnO_2-3, AC-3, and $BaTiO_3$-3 filters. As expected, bare PU foam had nearly no removal efficiency for formaldehyde, but the filter MnO_2-3 showed a relatively high removal efficiency of 64.3%. Similar to the ozone removal mechanism, charged formaldehyde molecules are captured by polarized fibers owing to the electric force[51] and then are catalyzed by MnO_2 loaded on the fibers.[52] However, as filter AC-3 showed only 4.9% removal efficiency, we suspected that in an EAHC filter with ultralow pressure drop (large pore size and porosity), catalyst loading might be more effective than the adsorbent for airborne formaldehyde removal.

4.5. Comparison with Other Studies. Figure 4a illustrates the contributions of mechanical, charging, and polarizing effects to the overall filtration efficiency of different fibers.

- Conventional filters usually remove PM from airflow mechanically by the combined effects of Brownian diffusion, interception, and inertial impaction.[53] Thus, they consume the largest pressure drop among all types of filters owing to the large filling ratio.
- By enlarging the electrostatic effect between the fibers and airborne PM, researchers developed electret filters[20] and ion-assisted filters[21−25] in which either filter or airborne PM is charged. Therefore, the insufficient electrostatic effect makes electret filters and ion-assisted filters still rely on mechanical effect and consume considerable pressure drop.
- An EAA coarse filter is developed with airborne PM charged by corona discharging and filter fibers charged by an external electrical polarizing field. Therefore, the EAA coarse filter realizes a lower pressure drop with maintained filtration efficiency. However, the charging and polarizing voltages in an EAA coarse filter are limited by safety and energy consumption problems. Too high voltages not only lead to air breakdown but also produce hazardous byproducts such as ozone.
- To approach an ultralow-pressure-drop filtration, new filter materials with desirable dielectric properties are designed in this study. The fiber loaded with large ε_r HCs will generate a great amount of charge on its surface while being installed in a polarizing field. Therefore, they have a strong attraction to precharged airborne PM and show high filtration efficiency with ultralow pressure drop.

The experimental results from reported literature and commercial filters also support this conclusion. As shown in Figure 4b, the EAHC filters have remarkably lower pressure drop than those in both literature reported and commercial air filters while achieving similar filtration efficiency. Besides, previous studies mainly focused on thin (membrane) filters, which have poor dust-holding capacity. The bulk foam-structured HC filters in this study will potentially show a lower speed in increase of the pressure drop and a higher total dust-holding capacity when considering long-term performance. Furthermore, the HC filters are also designed to be multifunctional for ambient particle, ozone, and formaldehyde removal by being loaded with different adsorbent (AC) and catalyst (manganese dioxide) materials.

5. CONCLUSIONS

In summary, we demonstrated dielectric HC filters with ultralow pressure drop for efficient electrostatic multifunctional air filtration. The idea is, while loading normal filters with high-ε_r HCs, the dielectric filter material in a polarizing field would generate a great amount of charge on its surface, have a strong attraction to precharged airborne particles, and result in high filtration efficiency. We observed *via* a CCD camera that the migration speeds of smoke particles on the polarized HC fiber exceeded those on the unpolarized HC fiber by a factor of 6 and formed particle chains specifically upon the high-ε_r HCs.

We loaded high-ε_r HCs (MnO_2, AC, ZnO, CuO, and $BaTiO_3$) on PU foams using a fast and large-scale roll-to-roll gel squeezing method. Installed in an EAHC air filtration module, the filter ZnO-3 can remove $PM_{0.3-0.5}$ and $PM_{0.5-1}$ from ambient air with single-pass filtration efficiencies of 87.0 and 89.2%, respectively, and a pressure drop of 3.8 Pa at 1.1 m/s filtration velocity.

The dielectric HC filters not only overcome the intrinsic conflict between high particle removal efficiency and low wind pressure drop but also simultaneously remove indoor gaseous pollutants. We suggest filter MnO_2-3 because it has less than 5 Pa pressure drop and relatively high removal efficiency for primary indoor air pollutants: 84.2% for $PM_{0.3-0.5}$, 85.9% for $PM_{0.5-1}$, 53.8% for ambient ozone, and 64.3% for formaldehyde.

■ ASSOCIATED CONTENT

Supporting Information

The Supporting Information is available free of charge at https://pubs.acs.org/doi/10.1021/acsami.0c07447.

Performance test method of the EAHC air filtration module and calculation methods (PDF)

HC filter washed by hands (MP4)

Particle movement toward the HC fiber at zero voltage (MP4)

Particle movement toward the HC fiber at +5kV (MP4)

■ AUTHOR INFORMATION

Corresponding Authors

Hao Wang − *College of Engineering, Peking University, Beijing 100871, China;* orcid.org/0000-0003-2882-3802; Email: hwang@coe.pku.edu.cn

Jinhan Mo − *Department of Building Science, Tsinghua University, Beijing 100084, China; Beijing Key Laboratory of Indoor Air Quality Evaluation and Control, Beijing 100084, China;* orcid.org/0000-0002-3178-6507; Email: mojinhan@tsinghua.edu.cn

Authors

Enze Tian − *Department of Building Science, Tsinghua University, Beijing 100084, China; Beijing Key Laboratory of Indoor Air Quality Evaluation and Control, Beijing 100084, China;*

https://dx.doi.org/10.1021/acsami.0c07447
ACS Appl. Mater. Interfaces 2020, 12, 29383−29392

Department of Nuclear Science and Engineering, Massachusetts Institute of Technology, Cambridge, Massachusetts 02139, United States; orcid.org/0000-0001-6410-5360

Fanxuan Xia − *Department of Building Science, Tsinghua University, Beijing 100084, China; Beijing Key Laboratory of Indoor Air Quality Evaluation and Control, Beijing 100084, China*

Jiandong Wu − *College of Engineering, Peking University, Beijing 100871, China*

Yinping Zhang − *Department of Building Science, Tsinghua University, Beijing 100084, China; Beijing Key Laboratory of Indoor Air Quality Evaluation and Control, Beijing 100084, China;* orcid.org/0000-0001-9175-7890

Ju Li − *Department of Nuclear Science and Engineering and Department of Materials Science and Engineering, Massachusetts Institute of Technology, Cambridge, Massachusetts 02139, United States;* orcid.org/0000-0002-7841-8058

Complete contact information is available at: https://pubs.acs.org/10.1021/acsami.0c07447

Author Contributions

The manuscript was written through the contributions of all authors. All authors have approved the final version of the manuscript.

Notes

The authors declare no competing financial interest.

■ ACKNOWLEDGMENTS

The research was supported by the National Key Research and Development Program of China (no. 2016YFC0207103) and the National Natural Science Foundation of China (nos. 51722807, 51521005 and 51976001). The authors would like to thank the support provided by the China Scholarship Council (CSC) (no. 201906210128) during a visit of Enze Tian to the Massachusetts Institute of Technology.

■ ABBREVIATIONS

AC, activated carbon
BET, Brunauer Emmett Teller
CCD, charged coupled device
CMC-Na, sodium carboxymethyl cellulose
CQF, comprehensive quality factor
EAA filter, electrostatically assisted air filter
EAHC filter, electrostatically assisted heterocaking filter
EAMF, electrostatically assisted metal foam
EDS, energy dispersive spectrometer
HC, heterocaking
HVAC, heating, ventilation, and air conditioning
HVDC, high voltage direct current
MBTH, 3-methyl-2-benzothiazolinone hydrazone hydrochloride
PM, particulate matter
PTFE, polytetrafluoroethylene
PVDF, polyvinylidene fluoride
$PM_{2.5}$, particulate matter with aerodynamic diameters less than 2.5 μm
PM_{1}, particulate matter with aerodynamic diameters less than 1 μm, submicrometer particles
$PM_{0.3-0.5}$, particulate matter with aerodynamic diameters of 0.3−0.5 μm
$PM_{0.5-1}$, particulate matter with aerodynamic diameters of 0.5−1 μm
ppi, pores per inch
PU, polyurethane
QF, quality factor
SEM, scanning electron microscopy
VAE, vinyl acetate-ethylene
VOCs, volatile organic compounds

■ REFERENCES

(1) Younan, D.; Petkus, A. J.; Widaman, K. F.; Wang, X.; Casanova, R.; Espeland, M. A.; Gatz, M.; Henderson, V. W.; Manson, J. E.; Rapp, S. R.; Sachs, B. C.; Serre, M. L.; Gaussoin, S. A.; Barnard, R.; Saldana, S.; Vizuete, W.; Beavers, D. P.; Salinas, J. A.; Chui, H. C.; Resnick, S. M.; Shumaker, S. A.; Chen, J.-C. Particulate Matter and Episodic Memory Decline Mediated by Early Neuroanatomic Biomarkers of Alzheimer's Disease. *Brain* **2019**, *143*, 289.

(2) Nichols, E.; Szoeke, C. E. I.; Vollset, S. E.; Abbasi, N.; Abd-Allah, F.; Abdela, J.; Aichour, M. T. E.; Akinyemi, R. O.; Alahdab, F.; Asgedom, S. W.; Awasthi, A.; Barker-Collo, S. L.; Baune, B. T.; Béjot, Y.; Belachew, A. B.; Bennett, D. A.; Biadgo, B.; Bijani, A.; Bin Sayeed, M. S.; Brayne, C.; Carpenter, D. O.; Carvalho, F.; Catalá-López, F.; Cerin, E.; Choi, J.-Y. J.; Dang, A. K.; Degefa, M. G.; Djalalinia, S.; Dubey, M.; Duken, E. E.; Edvardsson, D.; Endres, M.; Eskandarieh, S.; Faro, A.; Farzadfar, F.; Fereshtehnejad, S.-M.; Fernandes, E.; Filip, I.; Fischer, F.; Gebre, A. K.; Geremew, D.; Ghasemi-Kasman, M.; Gnedovskaya, E. V.; Gupta, R.; Hachinski, V.; Hagos, T. B.; Hamidi, S.; Hankey, G. J.; Haro, J. M.; Hay, S. I.; Irvani, S. S. N.; Jha, R. P.; Jonas, J. B.; Kalani, R.; Karch, A.; Kasaeian, A.; Khader, Y. S.; Khalil, I. A.; Khan, E. A.; Khanna, T.; Khoja, T. A. M.; Khubchandani, J.; Kisa, A.; Kissimova-Skarbek, K.; Kivimäki, M.; Koyanagi, A.; Krohn, K. J.; Logroscino, G.; Lorkowski, S.; Majdan, M.; Malekzadeh, R.; März, W.; Massano, J.; Mengistu, G.; Meretoja, A.; Mohammadi, M.; Mohammadi-Khanaposhtani, M.; Mokdad, A. H.; Mondello, S.; Moradi, G.; Nagel, G.; Naghavi, M.; Naik, G.; Nguyen, L. H.; Nguyen, T. H.; Nirayo, Y. L.; Nixon, M. R.; Ofori-Asenso, R.; Ogbo, F. A.; Olagunju, A. T.; Owolabi, M. O.; Panda-Jonas, S.; Passos, V. M. d. A.; Pereira, D. M.; Pinilla-Monsalve, G. D.; Piradov, M. A.; Pond, C. D.; Poustchi, H.; Qorbani, M.; Radfar, A.; Reiner, R. C.; Robinson, S. R.; Roshandel, G.; Rostami, A.; Russ, T. C.; Sachdev, P. S.; Safari, H.; Safiri, S.; Sahathevan, R.; Salimi, Y.; Satpathy, M.; Sawhney, M.; Saylan, M.; Sepanlou, S. G.; Shafieesabet, A.; Shaikh, M. A.; Sahraian, M. A.; Shigematsu, M.; Shiri, R.; Shiue, I.; Silva, J. P.; Smith, M.; Sobhani, S.; Stein, D. J.; Tabarés-Seisdedos, R.; Tovani-Palone, M. R.; Tran, B. X.; Tran, T. T.; Tsegay, A. T.; Ullah, I.; Venketasubramanian, N.; Vlassov, V.; Wang, Y.-P.; Weiss, J.; Westerman, R.; Wijeratne, T.; Wyper, G. M. A.; Yano, Y.; Yimer, E. M.; Yonemoto, N.; Yousefifard, M.; Zaidi, Z.; Zare, Z.; Vos, T.; Feigin, V. L.; Murray, C. J. L. Global, Regional, and National Burden of Alzheimer's Disease and Other Dementias, 1990-2016: A Systematic Analysis for the Global Burden of Disease Study 2016. *Lancet Neurol.* **2019**, *18*, 88−106.

(3) Du, Y. X.; Xu, X. H.; Chu, M.; Guo, Y.; Wang, J. H. Air Particulate Matter and Cardiovascular Disease: the Epidemiological, Biomedical and Clinical Evidence. *J. Thorac. Dis.* **2016**, *8*, E8−E19.

(4) Loxham, M.; Davies, D. E.; Holgate, S. T. The Health Effects of Fine Particulate Air Pollution. *Br. Med. J.* **2019**, *367*, l6609.

(5) Deng, Q.; Deng, L.; Miao, Y.; Guo, X.; Li, Y. Particle Deposition in the Human Lung: Health Implications of Particulate Matter from Different Sources. *Environ. Res.* **2019**, *169*, 237−245.

(6) Zhou, M.; Wang, H.; Zeng, X.; Yin, P.; Zhu, J.; Chen, W.; Li, X.; Wang, L.; Wang, L.; Liu, Y.; Liu, J.; Zhang, M.; Qi, J.; Yu, S.; Afshin, A.; Gakidou, E.; Glenn, S.; Krish, V. S.; Miller-Petrie, M. K.; Mountjoy-Venning, W. C.; Mullany, E. C.; Redford, S. B.; Liu, H.; Naghavi, M.; Hay, S. I.; Wang, L.; Murray, C. J. L.; Liang, X. Mortality, Morbidity, and Risk Factors in China and its Provinces, 1990-2017: a Systematic Analysis for the Global Burden of Disease Study 2017. *Lancet* **2019**, *394*, 1145−1158.

(7) Delfino, R. J.; Sioutas, C.; Malik, S. Potential Role of Ultrafine Particles in Associations between Airborne Particle Mass and Cardiovascular Health. *Environ. Health Perspect.* **2005**, *113*, 934−946.

(8) Cao, Z.-G.; Yu, G.; Chen, Y.-S.; Cao, Q.-M.; Fiedler, H.; Deng, S.-B.; Huang, J.; Wang, B. Particle Size: A Missing Factor in Risk Assessment of Human Exposure to Toxic Chemicals in Settled Indoor Dust. *Environ. Int.* **2012**, *49*, 24−30.
(9) Strak, M.; Janssen, N. A. H.; Godri, K. J.; Gosens, I.; Mudway, I. S.; Cassee, F. R.; Lebret, E.; Kelly, F. J.; Harrison, R. M.; Brunekreef, B.; Steenhof, M.; Hoek, G. Respiratory Health Effects of Airborne Particulate Matter: The Role of Particle Size, Composition, and Oxidative Potential-the RAPTES Project. *Environ. Health Perspect.* **2012**, *120*, 1183−1189.
(10) Turner, M. C.; Jerrett, M.; Pope, C. A.; Krewski, D.; Gapstur, S. M.; Diver, W. R.; Beckerman, B. S.; Marshall, J. D.; Su, J.; Crouse, D. L.; Burnett, R. T. Long-term Ozone Exposure and Mortality in a Large Prospective Study. *Am. J. Respir. Crit. Care Med.* **2016**, *193*, 1134−1142.
(11) Day, D. B.; Xiang, J.; Mo, J.; Li, F.; Chung, M.; Gong, J.; Weschler, C. J.; Ohman-Strickland, P. A.; Sundell, J.; Weng, W.; Zhang, Y.; Zhang, J. Association of Ozone Exposure with Cardiorespiratory Pathophysiologic Mechanisms in Healthy Adults. *JAMA Intern. Med.* **2017**, *177*, 1344−1353.
(12) Xiang, J.; Weschler, C. J.; Mo, J.; Day, D.; Zhang, J.; Zhang, Y. Ozone, Electrostatic Precipitators, and Particle Number Concentrations: Correlations Observed in a Real Office during Working Hours. *Environ. Sci. Technol.* **2016**, *50*, 10236−10244.
(13) IARC. IARC Working Group on the Evaluation of Carcinogenic Risk to Humans. *IARC Monographs on the Evaluation of Carcinogenic Risks to Humans, Formaldehyde, 2-Butoxyethanol and 1-tert-Butoxypropan-2-ol*, 2006; Vol. *88*.
(14) Du, Z.; Mo, J.; Zhang, Y. Risk Assessment of Population Inhalation Exposure to Volatile Organic Compounds and Carbonyls in Urban China. *Environ. Int.* **2014**, *73*, 33−45.
(15) Souzandeh, H.; Molki, B.; Zheng, M.; Beyenal, H.; Scudiero, L.; Wang, Y.; Zhong, W.-H. Cross-linked Protein Nanofilter with Antibacterial Properties for Multifunctional Air Filtration. *ACS Appl. Mater. Interfaces* **2017**, *9*, 22846−22855.
(16) Souzandeh, H.; Johnson, K. S.; Wang, Y.; Bhamidipaty, K.; Zhong, W.-H. Soy-protein-based Nanofabrics for Highly Efficient and Multifunctional Air Filtration. *ACS Appl. Mater. Interfaces* **2016**, *8*, 20023−20031.
(17) Ripple, W. J.; Wolf, C.; Newsome, T. M.; Barnard, P.; Moomaw, W. R. World Scientists' Warning of a Climate Emergency. *Bioscience* **2019**, *70*, 8−12.
(18) Xia, T.; Bian, Y.; Zhang, L.; Chen, C. Relationship between Pressure Drop and Face Velocity for Electrospun Nanofiber Filters. *Energy Build.* **2018**, *158*, 987−999.
(19) Stephens, B.; Novoselac, A.; Siegel, J. The Effects of Filtration on Pressure Drop and Energy Consumption in Residential HVAC Systems (RP-1299). *HVACR Res.* **2010**, *16*, 273−294.
(20) Wang, S.; Zhao, X.; Yin, X.; Yu, J.; Ding, B. Electret Polyvinylidene Fluoride Nanofibers Hybridized by Polytetrafluoroethylene Nanoparticles for High-efficiency Air Filtration. *ACS Appl. Mater. Interfaces* **2016**, *8*, 23985−23994.
(21) Agranovski, I. E.; Huang, R.; Pyankov, O. V.; Altman, I. S.; Grinshpun, S. A. Enhancement of the Performance of Low-efficiency HVAC Filters due to Continuous Unipolar Ion Emission. *Aerosol. Sci. Technol.* **2006**, *40*, 963−968.
(22) Park, J. H.; Yoon, K. Y.; Hwang, J. Removal of Submicron Particles Using a Carbon Fiber Ionizer-assisted Medium Air Filter in a Heating, Ventilation, and Air-conditioning (HVAC) System. *Build. Environ.* **2011**, *46*, 1699−1708.
(23) Noh, K.-C.; Lee, J.-H.; Kim, C.; Yi, S.; Hwang, J.; Yoon, Y. H. Filtration of Submicron Aerosol Particles Using a Carbon Fiber Ionizer-assisted Electret Filter. *Aerosol Air Qual. Res.* **2011**, *11*, 811−821.
(24) Noh, K.-C.; Park, J.-H.; Jung, Y.-K.; Yi, S.; Hwang, J. Characteristics of Submicron-sized Aerosol Filtration and Pressure Drop of an Electret Filter Installed in an Air Diffuser in a Residential Apartment Unit. *Aerosol Air Qual. Res.* **2011**, *11*, 80−89.
(25) Shi, B.; Ekberg, L. E.; Truschel, A.; Gusten, J. Influence of Filter Fiber Material on Removal of Ultrafine and Submicron Particles Using Carbon Fiber Ionizer-assisted Intermediate Air Filters. *ASHRAE Trans.* **2012**, *118*, 602−611.
(26) Mermelstein, J.; Kim, S.; Sioutas, C. Electrostatically Enhanced Stainless Steel Filters: Effect of Filter Structure and Pore Size on Particle Removal. *Aerosol. Sci. Technol.* **2002**, *36*, 62−75.
(27) Choi, D. Y.; Jung, S.-H.; Song, D. K.; An, E. J.; Park, D.; Kim, T.-O.; Jung, J. H.; Lee, H. M. Al-coated Conductive Fibrous Filter with Low Pressure Drop for Efficient Electrostatic Capture of Ultrafine Particulate Pollutants. *ACS Appl. Mater. Interfaces* **2017**, *9*, 16495−16504.
(28) Choi, D. Y.; An, E. J.; Jung, S. H.; Song, D. K.; Oh, Y. S.; Lee, H. W.; Lee, H. M. Al-coated Conductive Fiber Filters for High-efficiency Electrostatic Filtration: Effects of Electrical and Fiber Structural Properties. *Sci. Rep.* **2018**, *8*, 5747.
(29) Tian, E.; Mo, J.; Li, X. Electrostatically Assisted Metal Foam Coarse Filter with Small Pressure Drop for Efficient Removal of Fine Particles: Effect of Filter Medium. *Build. Environ.* **2018**, *144*, 419−426.
(30) Tian, E.; Gao, Y.; Mo, J. Electrostatically Assisted Air Coarse Filtration for Energy Efficient Ambient Particles Removal: Long-term Performance in Real Environment and Influencing Factors. *Build. Environ.* **2019**, *164*, 106348.
(31) Tian, E.; Mo, J. Toward Energy Saving and High Efficiency through an Optimized Use of a PET Coarse Filter: The Development of a New Electrostatically Assisted Air Filter. *Energy Build.* **2019**, *186*, 276−283.
(32) Lee, J.-K.; Kim, S.-C.; Shin, J.-H.; Lee, J.-E.; Ku, J.-H.; Shin, H.-S. Performance Evaluation of Electrostatically Augmented Air Filters Coupled with a Corona Precharger. *Aerosol. Sci. Technol.* **2001**, *35*, 785−791.
(33) Feng, Z.; Long, Z.; Mo, J. Experimental and Theoretical Study of a Novel Electrostatic Enhanced Air Filter (EEAF) for Fine Particles. *J. Aerosol Sci.* **2016**, *102*, 41−54.
(34) Feng, Z.; Cao, S.-J. A Newly Developed Electrostatic Enhanced Pleated Air Filters towards the Improvement of Energy and Filtration Efficiency. *Sustain. Cities Soc.* **2019**, *49*, 101569.
(35) Sambudi, N. S.; Choi, H.-J.; Lee, M.-H.; Cho, K. Capture of Ultrafine Particles Using a Film-type Electret Filter with a Unipolar Charger. *Aerosol Air Qual. Res.* **2017**, *17*, 626−635.
(36) Han, K. S.; Lee, S.; Kim, M.; Park, P.; Lee, M. H.; Nah, J. Electrically Activated Ultrathin PVDF-TrFE Air Filter for High-efficiency PM1.0 Filtration. *Adv. Funct. Mater.* **2019**, *29*, 1903633.
(37) Shapiro, M.; Laufer, G.; Gutfinger, C. Electric Forces in Aerosol Filtration in Fibrous and Granular Filters - a Parametric Study. *Atmos. Environ.* **1983**, *17*, 477−484.
(38) Meyer, G. J. Polyurethane Foam: Dielectric Materials for Use in Radomes and Other Applications. https://www.generalplastics.com/wp-content/uploads/2016/11/White-Paper-PU-Foam-Dielectric-Materials-for-Use-in-Radomes-and-Other_Applications.pdf (accessed December, 2019).
(39) Clipper Controls Inc. Dielectric Constant Values. http://www.clippercontrols.com/pages/Dielectric-Constant-Values.html (accessed November, 2019).
(40) Shkal, F.; Lopez, S. G.; Slocombe, D.; Porch, A. Microwave Characterization of Activated Carbons. *J. Comput. Commun.* **2017**, *6*, 112.
(41) Langton, N. H.; Matthews, D. The Dielectric Constant of Zinc Oxide over a Range of Frequencies. *Br. J. Appl. Phys.* **1958**, *9*, 453−456.
(42) Rosa, A.; Tulli, D.; Castera, P.; Gutierrez, A. M.; Griol, A.; Baquero, M.; Vilquin, B.; Eltes, F.; Abel, S.; Fompeyrine, J.; Sanchis, P. Barium Titanate (BaTiO3) RF Characterization for Application in Electro-optic Modulators. *Opt. Mater. Express* **2017**, *7*, 4328−4336.
(43) Simon-Seveyrat, L.; Hajjaji, A.; Emziane, Y.; Guiffard, B.; Guyomar, D. Re-investigation of Synthesis of BaTiO3 by Conventional Solid-state Reaction and Oxalate Coprecipitation Route for Piezoelectric Applications. *Ceram. Int.* **2007**, *33*, 35−40.
(44) Tian, E.; Mo, J.; Long, Z.; Luo, H.; Zhang, Y. Experimental Study of a Compact Electrostatically Assisted Air Coarse Filter for Efficient Particle Removal: Synergistic Particle Charging and Filter Polarizing. *Build. Environ.* **2018**, *135*, 153−161.

https://dx.doi.org/10.1021/acsami.0c07447
ACS Appl. Mater. Interfaces 2020, 12, 29383−29392

(45) Chen, H.; Mo, J.; Xiao, R.; Tian, E. Gaseous Formaldehyde Removal: A Laminated Plate Fabricated with Activated Carbon, Polyimide, and Copper Foil with Adjustable Surface Temperature and Capable of in situ Thermal Regeneration. *Indoor Air* **2019**, *29*, 469−476.
(46) Wei, X.; Zhou, H.; Chen, F.; Wang, H.; Ji, Z.; Lin, T. High-efficiency Low-resistance Oil-mist Coalescence Filtration Using Fibrous Filters with Thickness-direction Asymmetric Wettability. *Adv. Funct. Mater.* **2019**, *29*, 1806302.
(47) Peng, L. *Dust Removal Technology*; Chemical Industry Press: Beijing, 2014; pp 26−27.
(48) Fridman, A.; Kennedy, L. A. *Plasma Physics and Engineering*; Taylor & Francis, 2004.
(49) Liu, S.; Ji, J.; Yu, Y.; Huang, H. Facile Synthesis of Amorphous Mesoporous Manganese Oxides for Efficient Catalytic Decomposition of Ozone. *Catal. Sci. Technol.* **2018**, *8*, 4264−4273.
(50) Subrahmanyam, C.; Bulushev, D. A.; Kiwi-Minsker, L. Dynamic Behaviour of Activated Carbon Catalysts during Ozone Decomposition at Room Temperature. *Appl. Catal. B Environ.* **2005**, *61*, 98−106.
(51) Feng, Y.; Ling, L.; Nie, J.; Han, K.; Chen, X.; Bian, Z.; Li, H.; Wang, Z. L. Self-powered Electrostatic Filter with Enhanced Photocatalytic Degradation of Formaldehyde Based on Built-in Triboelectric Nanogenerators. *ACS Nano* **2017**, *11*, 12411−12418.
(52) Sidheswaran, M. A.; Destaillats, H.; Sullivan, D. P.; Larsen, J.; Fisk, W. J. Quantitative Room-temperature Mineralization of Airborne Formaldehyde Using Manganese Oxide Catalysts. *Appl. Catal. B Environ.* **2011**, *107*, 34−41.
(53) Paretsky, L.; Theodore, L.; Pfeffer, R.; Squires, A. M. Panel Bed Filters for Simultaneous Removal of Fly Ash and Sulfur Dioxide. *J. Air Pollut. Contr. Assoc.* **1971**, *21*, 204−209.
(54) Hanley, J. T.; Ensor, D. S.; Smith, D. D.; Sparks, L. E. Fractional Aerosol Filtration Efficiency of In-duct Ventilation Air Cleaners. *Indoor Air* **1994**, *4*, 169−178.
(55) Liu, J.; Zhang, H.; Gong, H.; Zhang, X.; Wang, Y.; Jin, X. Polyethylene/polypropylene Bicomponent Spunbond Air Filtration Materials Containing Magnesium Stearate for Efficient Fine Particle Capture. *ACS Appl. Mater. Interfaces* **2019**, *11*, 40592−40601.
(56) Zhang, S.; Tang, N.; Cao, L.; Yin, X.; Yu, J.; Ding, B. Highly Integrated Polysulfone/polyacrylonitrile/polyamide-6 Air Filter for Multilevel Physical Sieving Airborne Particles. *ACS Appl. Mater. Interfaces* **2016**, *8*, 29062−29072.
(57) Sun, Q.; Leung, W. W.-F. Enhanced Nano-aerosol Loading Performance of Multilayer PVDF Nanofiber Electret Filters. *Sep. Purif. Technol.* **2020**, *240*, 116606.
(58) Li, X.; Wang, C.; Huang, X.; Zhang, T.; Wang, X.; Min, M.; Wang, L.; Huang, H.; Hsiao, B. S. Anionic Surfactant-triggered Steiner Geometrical Poly(vinylidene fluoride) Nanofiber/nanonet Air Filter for Efficient Particulate Matter Removal. *ACS Appl. Mater. Interfaces* **2018**, *10*, 42891−42904.
(59) Hollingsworth & Vose. Technical Data for HVAC Filters. http://www.hollingsworth-vose.com/en/Products/Filtration-Media/Air-Filtration1/HVAC-filtration (accessed Feburary, 2020).

https://dx.doi.org/10.1021/acsami.0c07447
ACS Appl. Mater. Interfaces 2020, 12, 29383−29392